arXiv:0912.0592v1 [cond-mat.mes-hall] 3 Dec 2009

Spectral properties of photogenerated carriers in quantum well solar cells

U. Aeberhard

IEF-5 Photovoltaik, Forschungszentrum Jülich, D-52425 Jülich, Germany

---

Abstract

The use of low-dimensional structures such as quantum wells, wires or dots in the absorbing regions of solar cells strongly affects the spectral response of the latter, the spectral properties being drastically modified by quantum confinement effects. Due to the microscopic nature of these effects, a microscopic theory of absorption and transport is required for their quantification. Such a theory can be developed in the framework of the non-equilibrium Green's function approach to semiconductor quantum transport and quantum optics. In this paper, the theory is used to numerically investigate the density of states, non-equilibrium occupation and corresponding excess concentration of both electrons and holes in single quantum well structures embedded in the intrinsic region of a *p*-*i*-*n* semiconductor diode, under illumination with monochromatic light of different energies. Escape of carriers from the quantum well is considered via the inspection of the spectral photocurrent at a given excitation energy. The investigation shows that escape from deep levels may be inefficient even at room temperature.

Key words: quantum well solar cell, non-equilibrium Green's functions, quantum transport, photogeneration, tunneling escape, thermionic emission
PACS: 72.20.Jv, 72.40.+w, 73.21.Fg, 73.40.Kp, 78.67.De

---

1. Introduction

Efficient carrier escape from the quantum wells is one of the main premises for high performance of quantum well solar cells (QWSC), since for a contribution to photocurrent, the carrier sweep-out rate must exceed the recombination rate in the well. An advanced understanding of the escape mechanisms is thus indispensible for further optimization of such devices. To study carrier escape processes in QWSC, combined temperature and bias dependent photoluminescence and photocurrent measurements on *p*-*i*-*n* diodes including single quantum wells (SQW) in the intrinsic region were performed [1, 2, 3, 4, 5]. From the experimental results, two principle escape mechanisms were identified: thermal emission over [6] and tunneling through the confining barrier, where the latter can be assisted thermally or by scattering with phonons [7] or ionized impurities [8]. Both mechanisms depend on material properties and design parameters like width and height of the barriers as well as on external conditions like terminal voltage and temperature. In the case of thermionic emission, the escape rate increases with lower barrier and higher temperature, where the field dependence enters via the barrier height. Tunneling escape is determined via the quantum-mechanical transmission through the finite height barrier and increases with decreasing barrier thickness, as a consequence of weaker confinement that leads to broader levels corresponding to a shorter lifetime, and growing fields enabling Fowler-Nordheim tunneling by lowering the effective barrier height. At very high fields corresponding to reverse bias condition, carrier escape is found to be maximum, which is explained by the effective barrier being both narrow and low. At low fields corresponding to forward bias, i.e. for the situation that is relevant for photovoltaic operation, three temperature regimes with specific prevailing carrier escape channels have been established. At very low temperature, tunneling dominates, since on the one hand, there is no significant thermal population of higher levels near the top of the well that would allow thermal emission, and on the other hand the coherence length is increased. At intermediate temperature (100-200 K), tunneling becomes thermally assisted, via phonons or ionized impurity scattering. Finally, at the high (room) temperatures, escape was found to be dominated by thermionic emission, leading in many cases to an internal quantum efficiency close to unity [1, 9].

The experimental investigation of carrier escape from SQW was supplemented by a number of modelling approaches with increasing complexity, based on semiclassical pictures of thermionic emission and quantum mechanical descriptions of tunneling escape in terms of the barrier transmission function, which together allowed the determination of a carrier escape rate [1, 7, 10, 11]. However, these models share a set of shortcomings that have not been adressed properly since then. For instance, approximate models for the density of states were used, with abrupt dimensionality transition at the top of the well or even neglecting the lower dimensionality of the quantum well states. The confinement levels were determined without proper consideration of the quantum well in-plane, or transverse, dispersion. For the occupation of the confinement levels, the quasi-Fermi level was chosen to lie on the lowest level in the well, which is only true at large enough forward bias, and was not determined in function of the photoexcitation characteristics. Moreover, even though the effects of electron-phonon scattering on tunneling and occupation of higher-lying states in the well were considered in a few cases on a microscopic basis, they were not incorporated in a transport model beyond the rate equation level.

In this paper, we adress the issue of photocurrent generation in SQW *p-i-n* diodes on the basis of the Non-equilibrium Green's function (NEGF) formalism, a microscopic quantum-kinetic theory dating back to Keldysh [12], Kadanoff and Baym [13]. Within the framework of this theory, many of the limiting assumptions inherent to the quasiclassical Boltzmann picture can be relaxed, and energy resolved information is obtained for most of the relevant quantities. It allows for a combination of quantum mechanical descriptions of the electronic structure and the interactions of the many-body system composed of electrons, holes, photons and phonons with a theory of transport in open quantum systems, including both coherent and incoherent transport processes, and is therefore well suited for the investigation of the problem at hand where electron-hole pair photogeneration and carrier-phonon scattering have to be treated on equal footing with tunneling transport.

The paper is organized as follows. After a brief review of the theoretical model in the following section, we present and discuss the numerical results for the excess carrier density, the corresponding occupation function and the local photocurrent spectrum for different excitation energies in the range of the quantum well absorption.

2. Microscopic model of QWSC

The analysis in the present work relies on the microscopic theory of quantum well solar cells as discussed in detail in Ref. [14], which is based on the steady state non-equilibrium Green's function formalism. Since within this framework, the determination of the optical and electronic properties of a device differ considerably from the semiclassical macroscopic continuum approach conventionally used in photovoltaics, a brief sketch of the method shall be presented here.

2.1. The NEGF formalism

In the approach under discussion, physical quantities of interest, such as spectral density or current, are determined via the calculation of the steady-state non-equilibrium Green's functions for the charge carriers. These quantities are defined as non-equilibrium quantum statistical ensemble averages of pairs of single particle field operators. The retarded Green's function $G^{R}(\mathbf{r},t;\mathbf{r}',t')$, which provides e.g. the local density of states, and the correlation functions $G^{\lessgtr}(\mathbf{r},t;\mathbf{r}',t')$ providing density and current for electrons and holes, respectively, are obtained via the solution of the corresponding equations of motion, which for steady state ($t-t'\rightarrow E$) read[1]

$$\begin{aligned} G^{R(A)}(\mathbf{r}_1,\mathbf{r}_{1'};E) =& G_0^{R(A)}(\mathbf{r}_1,\mathbf{r}_{1'};E)+\int d^3r_2\int d^3r_3 G_0^{R(A)}(\mathbf{r}_1,\mathbf{r}_2;E)\\ &\times\Sigma^{R(A)}(\mathbf{r}_2,\mathbf{r}_3;E)G^{R(A)}(\mathbf{r}_3,\mathbf{r}_{1'};E), \qquad (1)\\ G^{\lessgtr}(\mathbf{r}_1,\mathbf{r}_{1'};E) =& \int d^3r_2\int d^3r_3 G^{R}(\mathbf{r}_1,\mathbf{r}_2;E)\Sigma^{\lessgtr}(\mathbf{r}_2,\mathbf{r}_3;E)G^{A}(\mathbf{r}_3,\mathbf{r}_{1'};E), \qquad (2) \end{aligned}$$

with the non-interacting retarded (advanced) Green's function given by

$$\left\{G_0^{R(A)}\right\}^{-1}(\mathbf{r},\mathbf{r}',E)=\left[E+(-)i\eta-H_0(\mathbf{r})-U(\mathbf{r})\right]\delta(\mathbf{r}-\mathbf{r}'),\quad \eta\rightarrow 0^{+}, \quad (3)$$

---

[1] We neglect the spin degrees of freedoms in the present discussion up to consideration of a factor of 2 corresponding to the sum over degenerate spin components.

where H_0 is the Hamiltonian of the non-interacting system and η provides the correct analytical properties. $\Sigma^{R,\lessgtr}$ denote the retarded self-energy and the scattering functions, respectively, and are composed of two contributions, due to the contacts and due to interactions within the active device. The effects of open boundaries and carrier injection from contact reservoirs are included via the boundary self-energies $\Sigma_B^{R,\lessgtr}$, which are determined by the bulk Bloch states of the electrodes that are occupied according to the chemical potential of the contact. The interaction of electrons and holes with phonons and photons is considered perturbatively via corresponding self-energy terms $\Sigma_{int}^{R,\lessgtr}$. Concerning the matter-light coupling, the dipole approximation for a monochromatic single-mode photon field is used for the optical excitation, and the coupling to a continuum for isotropic radiative emission. Elastic scattering by acoustic phonons is included in the deformation potential formulation, and the inelastic coupling to polar optical phonons is described via the Fröhlich Hamiltonian of the harmonic approximation.

Together with the expressions for the self energies from boundaries and interactions, which are calculated exactly (boundaries) or perturbatively within self-consistent first Born approximation (interactions) and depend linearly on the carrier Green's functions, and the macroscopic Poisson equation

$$\epsilon_0\nabla_{\mathbf{r}}\left[\epsilon(\mathbf{r})\nabla_{\mathbf{r}}U(\mathbf{r})\right]=n(\mathbf{r})-p(\mathbf{r})-N_{dop}(\mathbf{r}),\tag{4}$$

relating the Hartree potential U to doping density N_{dop} and the carrier densities derived from the Green's functions, relations (1) and (2) form a closed set of equations for the latter that have to be solved self-consistently.

2.2. Determination of physical quantities form NEGF

For the numerical investigation of quasi one-dimensional multilayer-systems such as multi quantum wells and superlattices, the Hamiltonian is represented in a discrete basis, e.g. consisting of a suitable combination of localized atomic orbitals $|\alpha, L, \mathbf{k}\rangle$, where α denotes the atomic orbitals, L the model layer and $\mathbf{k}$ the in-plane, or transverse, momentum. In this basis, the local density of states (LDOS) at layer L is given by

$$\mathscr{D}_L(E)=\sum_{\mathbf{k}}\mathrm{tr}\{A_{L;L}(\mathbf{k};E)\},\qquad A_{L;L}(\mathbf{k};E)=i\left[G^R_{L;L}(\mathbf{k};E)-G^A_{L;L}(\mathbf{k};E)\right],\tag{5}$$

where A is the spectral function and the trace is over orbital indices. The averaged electron (hole) density at layer L is

$$n_L=-\frac{2i}{\mathcal{A}\Delta}\sum_{\mathbf{k}}\int\frac{dE}{2\pi}tr\{G^<_{L;L}(\mathbf{k};E)\},\qquad p_L=\frac{2i}{\mathcal{A}\Delta}\sum_{\mathbf{k}}\int\frac{dE}{2\pi}tr\{G^>_{L;L}(\mathbf{k};E)\},\tag{6}$$

where $\mathcal{A}$ denotes the cross section area and Δ the layer thickness. The current density passing from layers L to $L+1$ is

$$J^{n(p)}_{L,L+1} = \frac{2e}{\hbar\mathcal{A}} \sum_{\mathbf{k}} \int \frac{dE}{2\pi} tr\{t_{L;L+1} G^{<(>)}_{L+1;L}(\mathbf{k};E) - t_{L+1;L} G^{<(>)}_{L;L+1}(\mathbf{k};E)\}. \quad (7)$$

It is possible to define an effective local carrier distribution function $\tilde{f}_L(E)$ via

$$\tilde{f}_L(E) \equiv \frac{\rho_L(E)}{\mathscr{D}_L(E)} = \frac{\sum_{\mathbf{k}} \mathrm{tr}\{-iG^{<}_{L;L}(\mathbf{k};E)\}}{\sum_{\mathbf{k}} \mathrm{tr}\{A_{L;L}(\mathbf{k};E)\}}, \quad (8)$$

where $\rho_L(E)$ is the spectral density at layer L.

3. Numerical results

The following results for bulk and SQW *p*-*i*-*n*-diodes were all obtained using the two-band tight-binding sp_z-Hamiltonian discussed in Ref. [14], with the same set of parameters corresponding to a GaAs-Al$_x$Ga$_{1-x}$As heterostructure, but with energy gaps of 0.5 eV (well) and 0.9 eV (barrier), and band offset (=barrier height) of 0.25 eV in the conduction band and 0.25 eV in the valence band. The active device region, where interactions are considered, includes a SQW of 25 monolayers (ML) width and 5 ML adjacent barrier material. The contacts are formed by 50 ML high bandgap material with strong doping ($N_{d,a} = 10^{18}$ cm^{-3}). Between contact and active device, intrinsic buffer regions of 60 ML are inserted. The calculations are performed at 300 K and an illumination intensity of 1 kW/m^2.

3.1. Photogenerated excess carrier density

Fig. 1 shows the photogenerated excess carrier density $\delta n = n_{light} - n_{dark}$ for the SQW diode and several photon energies lying in the range of the confinement level separation between the two band gap values, such that the contact and lead regions are non-absorbing.

Owing to the localized nature of the states which are occupied, the fraction of the carriers that leaks out of the well is small, especially in the case of the electrons, which are more confined than the holes. The higher electron concentration is a consequence of the longer escape times of the electrons resulting from this stronger confinement. It is further interesting to notice that while the hole concentration follows the increase in photocurrent with larger photon energy, this is not the case for the electron concentration. This observation is explained by the stronger increase in escape channels for electrons at higher excitation energies as compared to the situation of the holes, where the enhancement sets in at lower energies, i.e. the slow escape of electrons at intermediate excitation energies leads to charge build-up in the well.

3.2. *Non-equilibrium occupation of confinement levels*

To investigate the occupation of available states by the photogenerated excess carriers, the spectral density $\delta\rho_L(E)$ of the latter is computed for different excitation energies. In Fig. 2, the photogenerated excess carrier spectral density for illumination with $E_{phot} = 0.568\ eV$ (bound state transition) is displayed. At this low energy, the photogenerated carriers occupy only the lowest subband. This means that not only the dark carrier concentration, but also the photogenerated carrier density is strongly localized in energy around the lowest level, and the occupation of higher and lower energy states via phonons produces pronounced satellite peaks, both in the conduction band well and the valence band well.

The photogenerated excess carrier spectral density for illumination with $E_{phot} = 0.888\ eV$ (quasi-bound state transition) is shown in Fig. 3. At this photon energy, states high in the quantum well that are broad due to fast escape are occupied by the photoexcitation process. Subsequent carrier relaxation via emission of phonons leads to the occupation of the lower confinement levels, which then provide the main contribution to the spectral density. Due to the width of the states of initial occupation, the final excess carrier spectrum exhibits only smooth features. This smoothing of the phonon satellite peaks with increasing excitation energy and the accumulation of density on the lowest confinement levels can also be seen in Fig. 4, which shows a cut of the spectral excess carrier concentration at the position of its maximum in the well. What is interesting to notice in this figure is the large difference in the degree of thermionic emission between electrons and holes: while the excess carrier density in the valence band has a tail that extends far above the effective barrier edge at $E_V \sim 0.35\ eV$, the corresponding density is very low in conduction band

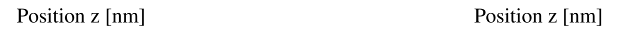

Figure 1: Photogenerated excess carrier density for different photon energies at $V_{bias} = -0.01V$. The quantum well location is indicated by the band edges E_C and E_V, respectively. The electronic density exceeds the hole concentration due to stronger confinement and resulting slower carrier escape. While the electron density is largest at intermediate excitation energies due to the absence of efficient escape channels, the increase of the hole density closely follows the absorption, which at low energies grows step-like.

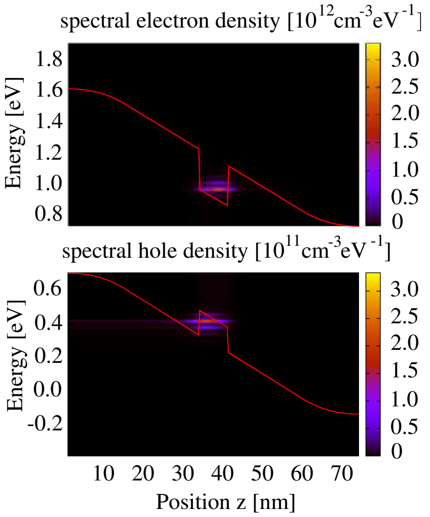

Figure 2: (Color online) Photogenerated excess carrier spectral density for illumination with $E_{phot} = 0.568\ eV$ (bound-state transition), at $V_{bias} = -0.01$ V. Interaction with phonons leads to the formation of distinct satellites peaking at the energy distance of an integer multiple of the phonon energy $\hbar\omega_{LO} = 0.036$ eV.

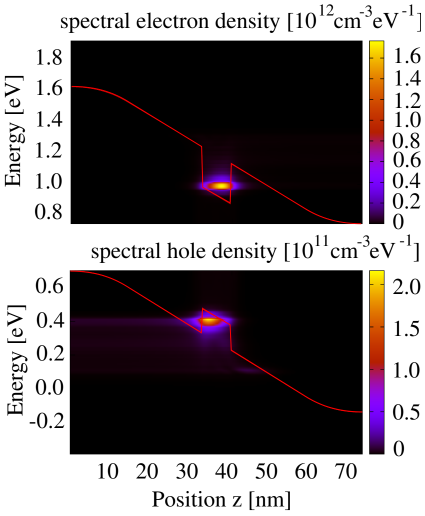

Figure 3: (Color online) Photogenerated excess carrier spectral density for illumination with $E_{phot} = 0.888\ eV$ (quasi-continuum transition), at $V_{bias} = -0.01$ V. The phonon peaks are no longer distinguishable due to larger broadening of the higher, less confined states which are occupied at this excitation energy.

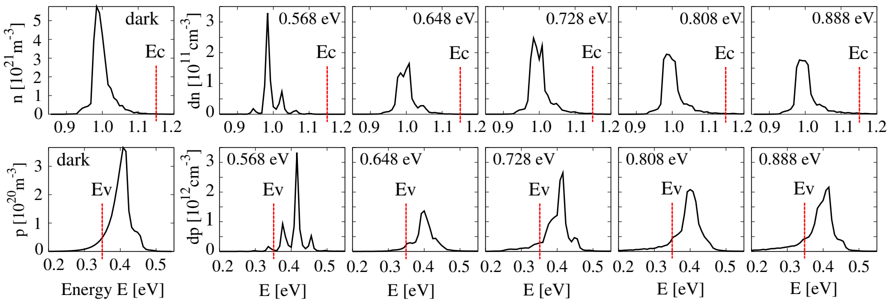

Figure 4: Spectral resolution of the excess carrier density for different photon energies (cut at the position of the maximum in the quantum well). For comparison, the carrier concentration in the dark is given for the same position in the quantum well. E_C and E_V indicate the effective well edges for electrons and holes, respectively. While the phonon satellite peaks get smoothened at higher excitation energies due to occupation of broadened states, the highest weight remains always on the lowest confinement level. Only the hole density shows a significant fraction at energies above the effective well edge E_V, which is required for efficient thermionic emission.

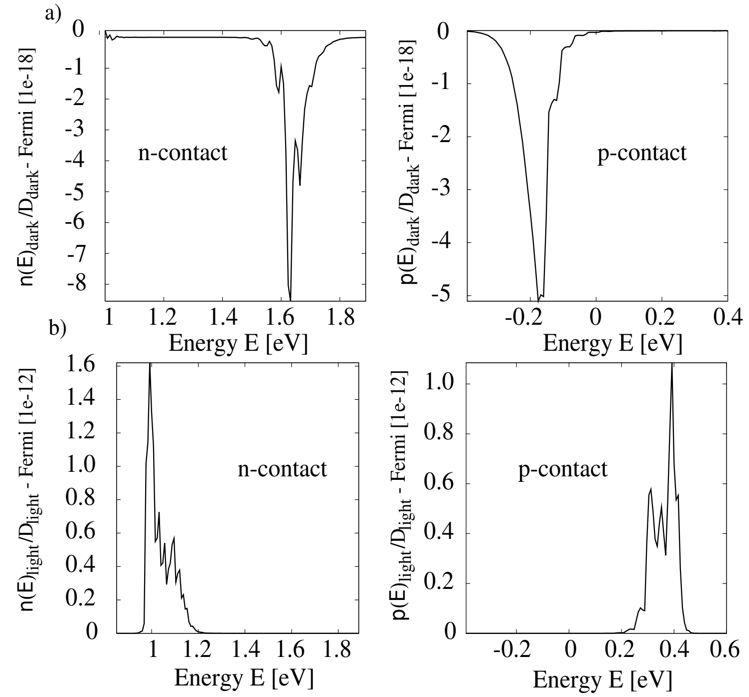

Figure 5: Distribution function $\tilde{f}_L(E) \equiv \rho_L(E)/\mathscr{D}_L(E)$ at the majority carrier contact ($L = N_z$ for electrons, $L = 1$ for holes) under small forward bias ($V = -0.01\ V$), in the dark and under illumination, with comparison to the equilibrium Fermi distribution $f_\mu(E)$ of the contacts with chemical potential μ: (a) deviation $\delta f = \tilde{f} - f_\mu$ from the equilibrium distribution in the dark, (b) deviation from equilibrium under illumination.

well at the effective barrier edge of $E_C \sim 1.15\ eV$, even at the highest excitation energies. The phonon satellite peaks get smoothed at higher excitation energies due to occupation of broadened states, but the highest weight remains always on the lowest confinement level, independent of the energy of the photon.

The occupation function corresponding to the excess carrier density is evaluated using relation (8). Fig. 5 shows this distribution at the majority carrier contact ($L = N_z$ for electrons, $L = 1$ for holes) under small forward bias ($V = -0.01\ V$), in the dark and under illumination, with comparison to the equilibrium Fermi distribution $f_\mu(E)$ of the contacts with chemical potential μ. In the dark, the only evidence of non-equilibrium giving rise to a deviation $\delta f = \tilde{f} - f_\mu$ from the equilibrium distribution is the signature of the leakage current from the opposite contact, which is characterized by a chemical potential μ' that differs from μ by the applied bias voltage, $\mu' = \mu + V_{bias}$. Under illumination, there is an additional deviation from equilibrium which reflects the distribution of the photogenerated excess carriers.

3.3. Photocurrent spectrum and carrier escape from quantum well states

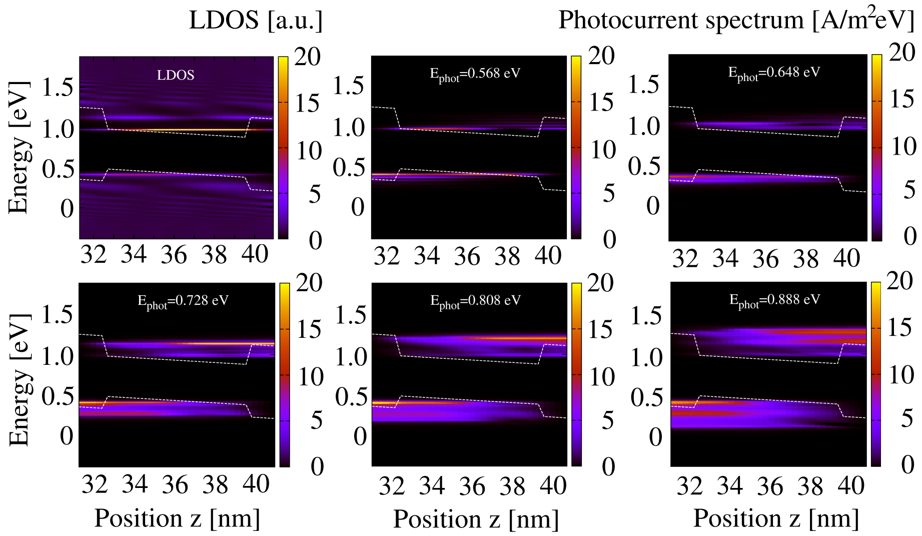

Figure 6: (Color online) Local density of states and energy resolved local photocurrent at $V_{bias} = -0.01\ V$, illustrating the carrier escape channels at different photon energies. Due to the presence of a high field, tunneling escape is possible even for the lower levels. At low excitation energy, transport is restricted to tunneling, whereas thermionic and phonon-assisted emission set in with the occupation of higher subbands.

Fig. 6 shows the local density of states and energy resolved local photocurrent in the active device region at $V_{bias} = -0.01\ V$, illustrating the carrier escape channels at different photon energies. At $E_{phot} = 0.568\ eV$, only the lowest subbands are occupied (see also Fig. 2). In the case of such a short structure and at low forward bias, escape from this level is possible via field enhanced tunneling. At $E_{phot} = 0.648\ eV$, the occupation is increased, but transport is still restricted to the lowest levels. This means that thermionic emission is not an efficient escape channel for deep levels, and the emission via phonon absorption is limited by the large separation of the subbands. At $E_{phot} = 0.728\ eV$, the occupation of the higher subbands has set in. From there, escape is efficient since the states are no longer strictly confined to the well, and thermionic emission is possible. The high level current increases further at $E_{phot} = 0.808\ eV$, and at $E_{phot} = 0.888\ eV$, additional quasi-bound states have started to contribute. The lower levels still contribute, but only a part of the subband carries current. An important result of this investigation is the observation that in the present case of very high fields, where tunneling from low levels is possible, this channel completely dominates the carrier escape, i.e. the contribution of thermionic emission is negligible in comparison.

4. Summary and conclusions

We have numerically investigated photocurrent generation in SQW *p*-*i*-*n* diodes using the NEGF-formalism, taking into account the correct density of states in the well for a two band model with parabolic transverse dispersion, the tunneling through the confining barrier and the scattering with acoustic and polar optical phonons. The occupation of the confined states is determined in function of external conditions such as energy and intensity of the photoexcitation and the separation of the contact Fermi-levels corresponding to a bias voltage. The computed excess carrier density strongly depends on the the excitation energy and thus on the level structure of the well. At the large fields that were investigated, tunneling is very efficient and represents the dominant escape channel. At low photon energies, where only the lowest subbands are partially populated, thermal occupation of higher states does not contribute significantly to the photocurrent from the well.

While for this qualitative discussion, an oversimplistic band structure model was used, a more accurate, atomistic approach is required to quantitatively model carrier escape, taking into account the non-parabolic and anisotropic transverse dispersion of the confinement levels at all energies in the well. For a proper description of carrier heating, confinement effects should also be considered for the phonons. While this gives a more accurate picture of the carrier escape, it is still necessary to consider on the same level also the recombination mechanisms that compete with it, i.e. extend the discussion to nonradiative recombination, in order to obtain a realistic internal quantum efficiency determining the effectiveness of the system in photovoltaic applications.

Acknowledgements

The author acknowledges financial support from the Institute of Theoretical Physics at ETH Zurich during the initial stage of this work.

References

References

[1] J. Nelson, M. Paxman, K. W. J. Barnham, J. Roberts, and C. Button, IEEE J. Quantum Electron. 29, 1460 (1993)

[2] G. Thucydides, J. M. Barnes, E. Tsui, K. W. J. Barnham, C. C . Phillips, T.S. Cheng, and C. T. Foxon, Semicond. Sci. Technol. 11, 331 (1996)

[3] J. Barnes, E. S. M. Tsui, K. W. J. Barnham,S. C. McFarlane, C. Button and J. S. Roberts, J. Appl. Phys. 81, 892 (1997)

[4] A. Zachariou, J. Barnes, K. W. J. Barnham, J. Nelson E. S. M. Tsui, J. Epler, and M. A. Pate, J. Appl. Phys. 83, 881 (1998)

[5] S. C. McFarlane,J. Barnes,K. W. J. Barnham, E. S. M. Tsui, C. Button, and J.S. Roberts, J. Appl. Phys. 86, 5109 (1999)

[6] H. Schneider and K. v. Klitzing, Phys. Rev. B 38, 6160 (1988)

[7] A. Larsson, P. Andrekson, S. Eng, and A. Yariv, IEEE J. Quantum Electron. 24, 787 (1988)

[8] A. Fox, D. Miller, G. Livescu, J. Cunningham, and W. Jan, IEEE J. Quantum Electron. 27, 2281 (1991)

[9] Y. Yazawa, T. Kitatani, J. Minemura, K. Tamura and T. Warabisako, Record of the 24th IEEE Photovoltaic Specialists Conference 2, 1878 (1994)

[10] J. Barnes, PhD thesis, Imperial College, London UK, 1994.

[11] D. Moss, T. Ido and H. Sano,IEEE J. Quantum Electron. 30, 1015 (1994)

[12] L. Keldysh, Sov. Phys.-JETP. 20, 1018 (1965)

[13] L. P. Kadanoff and G. Baym, *Quantum Statistical Mechanics* (Benjamin, Reading, MA 1962)

[14] U. Aeberhard and R.H. Morf, Phys. Rev. B 77, 125343 (2008)